Influence of temperature and free edges on the mechanical properties of graphene

2013 Modelling Simul. Mater. Sci. Eng. 21 065017

(http://iopscience.iop.org/0965-0393/21/6/065017)

Modelling Simul. Mater. Sci. Eng. **21** (2013) 065017 (15pp) doi:10.1088/0965-3393/21/6/065017

Influence of temperature and free edges on the mechanical properties of graphene

M A N Dewapriya[1,2], A Srikantha Phani[1] and R K N D Rajapakse[2]

[1] Department of Mechanical Engineering, The University of British Columbia, Vancouver, BC, Canada
[2] School of Engineering Science, Simon Fraser University, Burnaby, BC, Canada

E-mail: mandewapriya@sfu.ca, srikanth@mech.ubc.ca and rajapaks@sfu.ca

Received 19 February 2013, in final form 2 June 2013
Published 12 August 2013
Online at stacks.iop.org/MSMSE/21/065017

Abstract

A systematic molecular dynamics simulation study is performed to assess the effects of temperature and free edges on the ultimate tensile strength and Young's modulus of a single-layer graphene sheet. It is observed that graphene sheets at higher temperatures fail at lower strains, due to the high kinetic energy of atoms. A numerical model, based on kinetic analysis, is used to predict the ultimate strength of the graphene under various temperatures and strain rates. As the width of a graphene reduces, the excess edge energy associated with free edge atoms induces an initial strain on the relaxed configuration of the sheets. This initial strain has a greater influence on the Young's modulus of the zigzag sheet compared with that of the armchair sheets. The simulations reveal that the carbon–carbon bond length and amplitude of intrinsic ripples of the graphene increases with temperature. The initial out-of-plane displacement of carbon atoms is necessary to simulate the physical behaviour of a graphene when the Nosé–Hoover or Berendsen thermostat is used.

(Some figures may appear in colour only in the online journal)

1. Introduction

Graphene emerged as one of the potentially strongest and stiffest materials for the reinforcement of composite materials [1–4] with a tensile strength of 130 GPa and a Young's modulus of 1 TPa [5]. Graphene-based nano-electromechanical systems (NEMS) for sensing applications [6–8] and ultra-high frequency resonators [9] have been demonstrated. Narrow graphene sheets (width ≈15 nm) are required in nanoscale devices such as resonators and transistors [9, 10].

Edges and interfaces present in a finite, narrow sheet can change the thermo-mechanical properties and even influence the stability of graphene. Using molecular dynamics (MD) simulations and a finite element model, Shenoy *et al* [11] showed that edge stresses introduce ripples in free standing graphene sheets, even without any thermal effects. Reddy *et al* [12],

using MD simulations, showed that the edges strongly influence the elastic properties of graphene sheets when the width is less than 8 nm. Bu *et al* [13] studied the mechanical behaviour of armchair graphene nanoribbons (GNRs) using MD simulations. According to their observations, the Young's modulus increases with width up to 4 nm and thereafter attains the value of bulk graphene. Lu and Huang [14] used molecular mechanics (MM) simulations to investigate the effects of edges on the equilibrium configurations of GNRs and found that compressive edge forces cause GNRs to extend along the direction of free edges. They also observed that the Young's modulus decreases with increasing width in both types of GNR (armchair and zigzag) up to 6 nm and then reaches the value of bulk graphene [15]. This observation is in contradiction to what was observed in [13]. This may be due to different potential fields used in the two simulations. A Tersoff potential was used in [13] while a reactive empirical bond order (REBO) potential was used in [15]. On the other hand, the simulations in [13] were performed at 300 K, while the simulation temperature is 0 K in [15]. Therefore, it is important to understand the effects of temperature on the Young's modulus of GNRs. A thorough understanding of the temperature effects is useful to design graphene-based devices operating at various temperatures.

It has been found that as temperature increases from 300 K to 900 K, the ultimate tensile strength (σ_{ult}) and the ultimate tensile strain (ε_{ult}) of an infinitely large armchair sheet decrease by around 20% and 30%, respectively [16]. The effects of temperature on the zigzag graphene has not been previously investigated. It is important to study the effects of temperature on both the zigzag and armchair graphene, which will give a complete picture on the temperature dependence of σ_{ult} and ε_{ult} of graphene. A study on the effects of temperature on the mechanical properties of an infinitely large graphene sheet sets a baseline for understanding the effects of edges at various temperatures.

This paper presents a comprehensive MD simulation study to investigate the effects of temperature as well as edges on the Young's modulus, σ_{ult}, and ε_{ult} of armchair and zigzag graphene. The paper is organized as follows. Section 2 gives an overview of the MD simulation set up. An investigation of the effects of temperature on Young's modulus, σ_{ult}, and ε_{ult} of infinitely large graphene sheets is presented in section 3. This is followed by a study of the effects of edges on the Young's modulus, σ_{ult}, and equilibrium configuration of GNRs at various temperatures in section 4. The final section gives conclusions.

2. MD simulations

The accuracy of a MD simulation mainly depends on the potential field, which is an empirically derived mathematical description of the potential energy of a system of interacting atoms. An adaptive intermolecular reactive empirical bond order (AIREBO) potential [17], implemented in the LAMMPS MD simulation package [18], is used in this study. The AIREBO potential is considered to be one of the best available to simulate hydrocarbon systems such as graphene since it considers both covalent and non-bonded interactions between atoms [12, 16, 19]. The potential consists of three parts as given below.

$$E^{\text{AIREBO}} = \frac{1}{2}\sum_{i}\sum_{j\neq i}\left[E_{ij}^{\text{REBO}} + E_{ij}^{\text{LJ}} + \sum_{k\neq i,j}\sum_{l\neq i,j,k} E_{ijkl}^{\text{tors}}\right], \tag{1}$$

where E^{AIREBO} is the total potential energy of a system of atoms and the indices i, j, k and l refer to individual atoms; E_{ij}^{REBO} is the REBO part, which represents the energy stored in the bond between atoms i and j; E_{ij}^{LJ} is the Lennard-Jones potential which considers the non-bonded interactions between atoms; and E_{ijkl}^{tors} includes the energy from torsional interactions between atoms.

The REBO part consists of the repulsive potential (V_{ij}^{R}) and the attractive potential (V_{ij}^{A}), which are combined using the bond order term (b_{ij}) as

$$E_{ij}^{\mathrm{REBO}} = f(r_{ij})\left(V_{ij}^{\mathrm{R}} + b_{ij}V_{ij}^{\mathrm{A}}\right), \tag{2}$$

where b_{ij} modifies the bond strength depending on the local bonding environment. The function $f(r_{ij})$ is called the cut-off function. The purpose of $f(r_{ij})$ is to limit the interatomic interactions to the nearest neighbours [20]. The originally suggested $f(r_{ij})$ in the REBO potential is given by

$$f(r_{ij}) = \begin{cases} 1, & r_{ij} < R^{(1)} \\ \left[1 + \cos\left[\frac{\pi(r_{ij}-R^{(1)})}{(R^{(2)}-R^{(1)})}\right]\right]/2, & R^{(1)} < r_{ij} < R^{(2)} \\ 0, & R^{(2)} < r_{ij}, \end{cases} \tag{3}$$

where r_{ij} is the bond length; $R^{(1)}$ and $R^{(2)}$ are the cut-off radii, which have the values of 1.7 Å and 2 Å, respectively. The values of the cut-off radii have been defined based on the first and second nearest neighbouring distances of hydrocarbons.

It has been observed that the cut-off function could lead to a nonphysical strain hardening in stress–strain curves of carbon nanostructures [21–23], whereas experiments [5] and *ab initio* calculations [24] do not show any strain hardening. Therefore, modified cut-off radii ranging from 1.9 Å to 2.2 Å [15, 19] have been used in the literature to eliminate the strain hardening. A detailed study is conducted on the effects of cut-off function of stress–strain curve of graphene and found that a fixed cut-off radius of 2 Å ($R^{(1)} = R^{(2)} = 2$ Å) eliminates the strain hardening. However, this truncated cut-off function makes the force field non-conservative, which prevents the bond reformation. Therefore, the cut-off radii should be carefully chosen when modelling bond reformation as well as crack propagation [23].

3. Effects of temperature

Graphene could be exposed to a temperature of 1000 K during the growth [25] and most of the graphene-based devices operate at room temperature. In this study, a graphene sheet with a size of 5 nm × 5 nm is subjected to uniaxial tension at temperatures ranging from 1 K to 800 K at intervals of 100 K to obtain a complete picture of temperature-dependent behaviour of graphene. Periodic boundary conditions (PBCs) are used in both in-plane directions to eliminate the effects of the edges. The strain rate and time step chosen are 0.001 ps^{-1} and 0.5 fs, respectively. The sheet is allowed to relax over a time period of 30 ps before applying strain. The pressure components along the in-plane directions are kept at zero during the relaxation using NPT ensemble implemented in LAMMPS. The NPT ensemble uses the Nosé–Hoover (NH) thermostat and barostat to control temperature and pressure, respectively. Surface ripples in suspended graphene sheets have been observed in experiments at room temperature [26–28]. The coefficient of thermal expansion (CTE) of graphene at 300 K was observed to be between $-6 \times 10^{-6}\,\mathrm{K}^{-1}$ and $-7 \times 10^{-6}\,\mathrm{K}^{-1}$ [26, 29]. Molecular dynamic studies are reported here on the configuration of free standing single-layer graphene sheets and their thermal expansion properties.

3.1. Influence of thermostat on equilibrium configuration of graphene

A graphene sheet of 5 nm × 5 nm is allowed to reach equilibrium over 75 ps at various temperatures raging from 1 K to 800 K. At each temperature, three simulations are performed using NH, Berendsen (Ber) and Langevin (Lan) thermostats to control the temperature. It is observed that both the NH and Ber thermostats induce a thermal expansion on the graphene

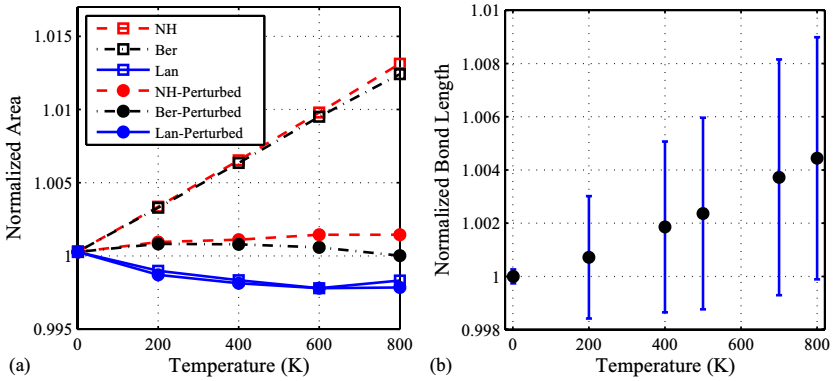

Figure 1. (*a*) Influence of thermostat on the equilibrium area of graphene. The areas have been normalized with respect to the area at 1 K (2554 Å^2). The standard deviation of the normalized areas, given by different thermostats at 800 K, is around 0.002. (*b*) Temperature dependence of bond length. The error bars indicate 10% of the standard deviation of the bond lengths. The bond lengths have been normalized with respect to the bond length at 1 K (1.397 Å).

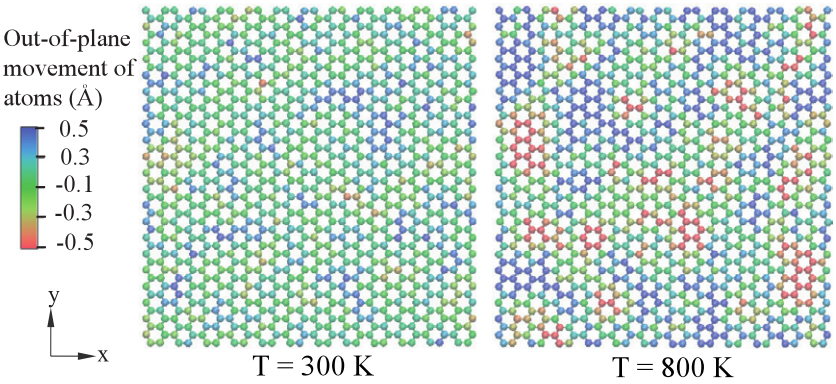

Figure 2. Ripples in graphene sheets of size 5 nm × 5 nm at equilibrium.

sheet shown in figure 1(*a*). The kinetic energy at higher temperatures makes graphene sheets have higher potential energy, which is achieved by increasing the bond lengths as shown in figure 1(*b*). However, this artefact thermal expansion disappears when an initial random displacement perturbation (≈0.05 Å) is induced to the atoms. It is found that the equilibrium areas of graphene in figure 1(*a*) do not depend on the amplitude of the initial perturbation. However, the amplitude of the ripples at the equilibrium configuration increases with the temperature as shown in figure 2. This reduces the effective thermal expansion even though the bond lengths increase with the temperature as shown in figure 1(*b*). It is also found that the failure strain without initial perturbation is around 7% less than that obtained with perturbation when the NH thermostat is used. This is due to the difference in the initial configuration of the two cases. However, this change in the failure strain results in a less than 1% change in the failure stress due to the softening of graphene at higher strains as explained in section 3.2.

The NH thermostat modifies the equation of motion using a friction factor [31, 32]. The NH equation can be written as

$$\frac{\mathrm{d}p_i}{\mathrm{d}t} = f_i - \mu p_i \tag{4}$$

Table 1. CTE of graphene at 300 K.

	CTE (10^{-6} K^{-1})	
Thermostat	Planar	Perturbed
Nosé–Hoover	16	0.78
Berendsen	15	−0.17
Langevin	−3.3	−3.0

where f_i is the force applied by the force field and p_i is the momentum of atom i; the friction factor μ is defined as

$$\frac{\mathrm{d}\mu\,(t)}{\mathrm{d}t} = \frac{N_\mathrm{f} k_\mathrm{B}}{Q}\left(T\,(t) - T_0\right), \tag{5}$$

where $T\,(t)$ and T_0 are the current and the desired temperatures, respectively; Q is the effective mass of the thermostat, which is given by $N_\mathrm{f} k_\mathrm{B} T_0 \tau_\mathrm{T}^2$; k_B is the Boltzmann constant; N_f is the total translational degrees of freedom of the system; τ_T is the specified time constant for temperature fluctuations. The value of τ_T should be around hundred time steps to achieve a smooth temperature transition.

The Ber thermostat [33] modifies the velocity of atoms by a scaling factor, λ, which is given as

$$\lambda = \sqrt{1 + \frac{\delta t}{\tau_T}\left(\frac{T_0}{T\,(t)} - 1\right)}, \tag{6}$$

where δt is the time step.

The Langevin (Lan) thermostat generates ripples in the equilibrium configuration of graphene even without an initial displacement perturbation, as indicated in figure 1(*a*). The Lan thermostat uses random fluctuating forces to describe the thermodynamics interactions [30]. These random forces induce out-of-plane motion of atoms, and thereby simulate the physical behaviour of graphene. The Lan equation can be written as

$$\frac{\mathrm{d}p_i}{\mathrm{d}t} = F_i + f_i - \gamma p_i, \tag{7}$$

where F_i is the random force with zero mean and $2\gamma m_i k_\mathrm{B} T_0$ of standard deviation; γ is the friction factor; m_i is the mass of atom i.

The bond lengths given in figure 1(*b*) do not depend on the thermostat or the initial perturbation. The calculated CTE of the carbon–carbon (C–C) bonds is 7.9×10^{-6} K^{-1}, which reasonably agrees with a value obtained from the first principle MD simulations (6.5×10^{-6} K^{-1}) in [34]. The calculated CTEs of graphene at 300 K are given in table 1. The table shows that the Lan thermostat gives CTEs closer to the experimental values, which are around -6×10^{-6} K^{-1}. CTEs given by the NH and Ber thermostats with initial perturbation are not significant compared with the experimental values.

The use of the NH and Ber barostats shows that the barostat does not have an influence on the initial configuration. Simulations using Lan and NH with ripples give similar stress–strain curves at 300 K. However, the NH thermostat implemented in LAMMPS is more computationally efficient than Lan thermostat. Therefore, the ensuing MD simulations are performed using the NH thermostat and barostat to control the temperature and pressure, respectively.

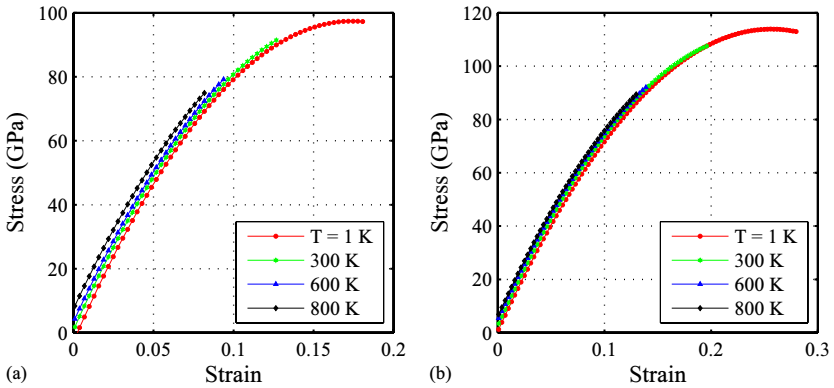

Figure 3. Stress–strain curves of (*a*) armchair and (*b*) zigzag graphene sheets at various temperatures.

3.2. Stress–strain behaviour

The stress of a graphene sheet (σ) is obtained from the gradient of potential energy (PE)-strain (ε) curve as

$$\sigma = \frac{1}{V}\frac{\partial(PE)}{\partial\varepsilon}, \tag{8}$$

where V is the volume of the graphene sheet, which is calculated assuming the thickness is 0.34 nm.

The comparison of the σ–ε relations of the armchair and zigzag sheets in figure 3 shows that the zigzag sheet is much stronger than the armchair sheet at a given temperature. The zigzag sheet has a failure strain up to 64% higher than that of the armchair sheet at a similar temperature, but results in only 21% higher strength due to softening with increasing strain. In armchair sheets, there are bonds along the straining direction, as shown in figure 6, and these bonds carry more strain compared with inclined bonds. All C–C bonds in zigzag sheets are inclined to the straining direction and a part of the strain is carried by changing the bond angles. Therefore, zigzag sheets can carry more strain compared with armchair sheets.

Figure 4(*a*) compares the variation of σ_{ult} and ε_{ult} with temperature. It can be seen that the effects of temperature are similar in both zigzag and armchair graphene sheets. The reduction of σ_{ult} is 23% and 27% and reduction in ε_{ult} is 54% and 59% in armchair and zigzag sheets, respectively. However, the effect of temperature on Young's modulus is not significant ($\approx$4%), as observed in [16].

The temperature and strain rate dependence of σ_{ult} and ε_{ult} can be numerically obtained using the Arrhenius formula [35] and Baileys principle [16]. The Arrhenius formula relates the lifetime (τ) as a function of stress and temperature (T) by the expression

$$\tau(T,t) = \frac{\tau_0}{n}\exp\left[\frac{U_0 - \gamma\sigma(t)}{k_{\text{B}}T}\right], \tag{9}$$

where τ_0 is the vibration period of atoms in solid; n is the number of sites available for state transition ; U_0 is the interatomic bond dissociation energy; $\gamma = qv$, where q and v are the coefficient of over stress and the activation volume, respectively; $\sigma(t)$ is the stress at time t; k_{B} is the Boltzmann constant.

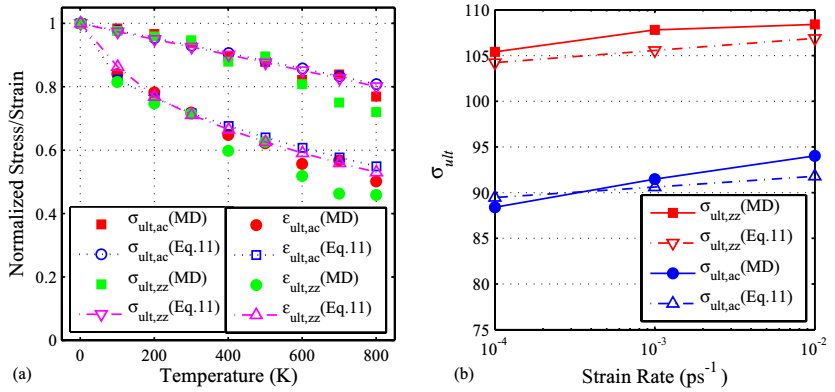

Figure 4. (*a*) Variations in normalized σ_{ult} and ε_{ult} of graphene with temperature. σ_{ult} and ε_{ult} are normalized with respect to those values at 1 K. Corresponding σ_{ult} are 97.3 GPa and 113.6 GPa for armchair (ac) and zigzag (zz) sheets, and the ε_{ult} are 0.173 and 0.273 for ac and zz sheets. (*b*) Comparison of the numerically predicted σ_{ult} with MD simulations at different strain rates.

The stress $\sigma(t)$ can take any arbitrary form as long as it fits the stress–strain data [16]. For a graphene sheet, $\sigma(t)$ can be expressed in terms of strain rate ($\dot{\varepsilon}$) and t as

$$\sigma(t) = a\left\{\ln\left[b\left(\dot{\varepsilon}t\right) + c\left(\dot{\varepsilon}t\right)^2 + 1\right]\right\}, \tag{10}$$

where a, b and c are constants; the product of a and b gives the Young's modulus of the sheet.

Bailey's principle states that fracture initiates when

$$\int_0^{t_f} \frac{\mathrm{d}t}{\tau(T,t)} = 1, \tag{11}$$

where t_f is the time taken to fracture. The strain rate and temperature-dependent lifetime is obtained by substituting equation (10) in equation (9). Then the failure time (t_f) is calculated solving equation (11) numerically. The failure stress is the stress at $t = t_f$, and the failure strain is given as $\varepsilon_{ult} = \dot{\varepsilon}t_f$.

Equation (11) is used to predict the failure stress and strain of both the armchair and zigzag graphene. U_0 is 4.95 eV; q is assumed as 1 for the armchair graphene and 97.3/113.6 for the zigzag graphene, where 97.3 and 113.6 are σ_{ult} (in GPa) of the armchair and zigzag graphene sheets at 1 K, respectively; v is used as 8.15 Å^3. The selected value of v is close to the representative volume of a carbon atom in graphene, which is 8.6 Å^3. τ_0 is taken as 5 fs [36]. The constant 'a' is 1012 GPa for both the armchair and zigzag graphene. The values of b and c are 1.1912 and −3.3473 for the armchair sheet and 0.9275 and −1.775 for the zigzag sheet. These constants are calculated from regression analysis of the stress–strain curves obtained from a MD simulation at 1 K.

Figure 4(*a*) shows that the numerical approach, outlined above, captures the σ_{ult} and ε_{ult} quite accurately at lower strain, but slightly overpredicts at higher temperatures. This is due to the fact that the constants a, b and c of equation (10) are obtained from the stress–strain curves at 1 K. Figure 3 indicates that the stress–strain curve of graphene has a small temperature dependence. Therefore, the constants a, b and c evaluated at 1 K are unable to predict the exact failure point at higher temperatures. However, the agreement between the numerical approach and MD simulations is acceptable.

Figure 4(*b*) compares the predicted failure stresses of graphene sheets at 300 K, under various strain rates, with the values obtained from MD simulations. The figure shows that the numerical approach is able to predict the failure stress with 3% accuracy. The most commonly

used strain rates in MD simulations are investigated in figure 4(*b*). It is impractical to use strain rates below 10^{-4} ps^{-1} due to the high computational cost.

3.3. Initial stress

Stress is inferred from the MD simulation by choosing a suitable measure. Different stress measures have been used in the literature [37]. Continuum stress measure introduced in equation (8) is shown in figure 3. It can be noted that the graphene sheets at zero strain have a residual tensile stress, and its magnitude depends on the temperature. All graphene sheets are properly relaxed before applying strain. Therefore, this initial stress could be due to the use of the continuum definition of stress in equation (8). To investigate this further, an alternative stress measure, namely virial stress, is calculated. This is one of the most commonly used atomistic stress measures which takes into account the temperature by considering the stress contribution from kinetic energy [38, 39]. It is defined as

$$\sigma_{ij} = \frac{1}{V}\sum_{\alpha}\left[\frac{1}{2}\sum_{\beta=1}^{N}\left(R_i^{\beta} - R_i^{\alpha}\right)F_j^{\alpha\beta} - m^{\alpha}v_i^{\alpha}v_j^{\alpha}\right], \tag{12}$$

where σ_{ij} is the virial stress; (i, j) are the directional indices (x, y and z); β is a number assigned to neighbouring atoms which varies from 1 to N; R_i^{α} is the position of atom α along direction i; $F_j^{\alpha\beta}$ is the force along direction j on atom α due to atom β; m^{α} is the mass of atom α; v^{α} is the velocity and V is the total volume.

It is found that the virial stress correctly calculates the initial stress as zero at different temperatures, whereas the values given by the continuum definition increase with temperature. The virial stress gives the initial stress as zero since it deducts the stress contribution from kinetic energy, as indicated in equation (12). MD simulations indicate that the change in kinetic and unstrained potential energies in various temperatures are similar and they increase linearly with the temperature. The change in energies per atom at 800 K is approximately 0.1 eV. The origin of the initial continuum stress is bond expansion, as shown in figure 1(*b*). The expansion of the bonds causes a sheet to have a slightly higher equilibrium potential energy compared with the lowest potential energy at higher temperatures, as shown in figure 5(*a*). The gradient of the potential energy–strain curve at the equilibrium configuration gives the initial stress. The gradient at the equilibrium configuration is approximately 0 at 1 K, whereas it is positive at 800 K, as shown in figure 5(*a*). The value of the gradient gradually increases as the temperature increases from 1 K to 800 K, causing the continuum initial stress to increase with temperature. The continuum initial stress values of the armchair and zigzag sheets are slightly different since the strain in C–C bonds depends on the bond orientations, as explained in section 3.2. Comparison of virial stress with continuum stress in figure 5(*b*) indicates that both stresses are almost equal up to a strain of 7%, and then virial stress gives higher values compared with continuum stress. The failure stress given by the virial stress is around 15% higher than that of continuum stress. We observe that other atomistic stress measures such as Hardy stress can equally be used [37]. Evaluating such atomistic stress measures is computationally intensive. Hence, continuum stress measure is used in this study.

4. Effects of edges

The effects of edges on Young's modulus and the ultimate tensile strength of GNRs are investigated by performing MD simulations on sheets with varying widths. The MD parameters are similar to those used in section 3. GNRs with the smallest widths are shown in figure 6.

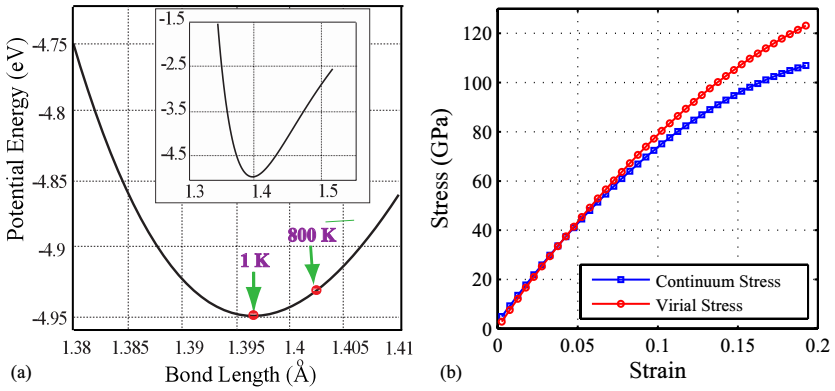

Figure 5. (*a*) Change in potential energy of a C–C bond with bond length obtained from a MD simulation with AIREBO potential. The arrows indicate the equilibrium positions at 1 K and 800 K. The inset shows the variation of potential energy in a wider range of bond lengths. (*b*) Comparison of virial stress and continuum stress measures of a zigzag graphene sheet at 300 K.

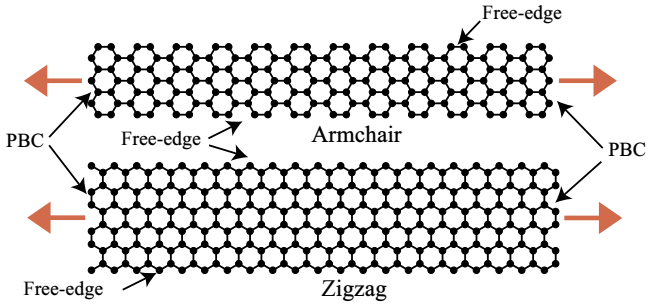

Figure 6. The smallest graphene sheet used for the study. The widths of the sheets are 0.7 nm and 1.1 nm for the armchair and zigzag sheets, respectively. The arrows (in red) indicate the straining direction.

PBCs are applied along the longitudinal direction, while keeping the transverse edges free. The length of the sheets is 5 nm. An elongation of the sheets along the longitudinal direction is observed as the sheets reach their equilibrium configurations. The elongation is significantly higher for narrow sheets.

4.1. Initial strain

Finite graphene sheets experience an elongation at the equilibrium configuration as a result of stress relaxation. In order to quantify the initial elongation of sheets, the initial strain (ε_0) is defined as

$$\varepsilon_0 = \frac{(l_{\text{eq}} - l_0)}{l_0}, \tag{13}$$

where l_{eq} is the equilibrium length of a sheet and l_0 is the equilibrium length of a sheet with an infinite width.

Figure 7 shows that narrow graphene sheets are subjected to significant ε_0, as high as 1%, and it asymptotically reaches zero as the width increases. The initial strain of zigzag graphene sheets are higher than that of the armchair sheet. This can be understood by considering the edge stress (τ), which arises from the difference of the energies in the edge and interior atoms.

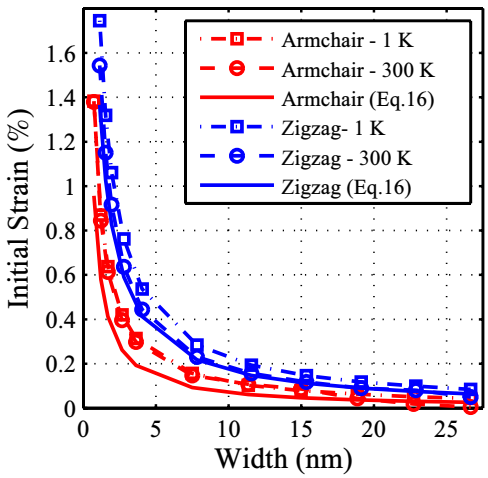

Figure 7. Variation of the initial strain of graphene sheets.

It has been found that τ of the zigzag edges are higher than that of the armchair edges [14]. The higher τ leads zigzag sheets to have higher ε_0 compared with armchair sheets, which has also been observed in a MM simulation study [14]. Temperature does not have an effect on the ε_0 of the armchair graphene, whereas it slightly decreases in the zigzag sheets when temperature increases from 1 K to 300 K.

The concept of surface stress of a three-dimensional crystal [41] can be used to calculate ε_0. The potential energy per unit length of a finite graphene sheet of width w, and under an axial strain ε can be expressed as [12]

$$U(\varepsilon, w) = U_0 + 2\tau\varepsilon + 2\left(\frac{1}{2}E_s\varepsilon^2\right) + \frac{1}{2}E\varepsilon^2 w, \tag{14}$$

where U_0 is the potential energy at zero strain; E and E_s are the bulk and the edge elastic moduli, respectively. The second and third terms in equation (14) are related to the edges. The factor of two in these edge terms accounts for the two free edges of a sheet. The stress $\sigma(\varepsilon, w)$ of the sheet can be obtained from the derivative of equation (14) with respect to ε as

$$\sigma(\varepsilon, w) = \frac{2\tau}{w} + \frac{2E_s\varepsilon}{w} + E\varepsilon. \tag{15}$$

It can be noted in equation (15) that the edge stress generates a strain (ε_0) at zero stress ($\sigma(\varepsilon, w) = 0$), which can be expressed as

$$\varepsilon_0 = \frac{-2\tau}{(2E_s + Ew)} = \frac{-2\tau}{wE_{\text{eff}}}, \tag{16}$$

where the effective Young's modulus (E_{eff}) is defined as $2E_s/w + E$.

Lu and Huang [14], using MM simulations with REBO potential, found that the value of τ is -2.6 nN and -1.36 nN for zigzag and armchair sheets, respectively. The values of τ in [14] and the E_{eff} calculated in this work are used to compute the ε_0 for various widths. The computed ε_0 agrees reasonably well with the values obtained from MD simulations at 1 K, as shown in figure 7.

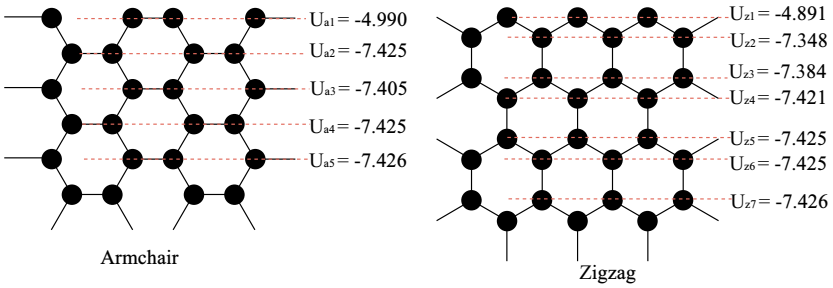

Figure 8. Variation of the potential energy of atoms with distance from the edge. $U_{a/z,i}$ (in eV) is the average potential energy of an atom of the armchair and zigzag graphene sheets in the ith row, which is indicated by a dashed line.

Table 2. Excess edge energy of graphene sheets by different methods.

Method	γ_{ac}	γ_{zz}
DFT (GPAW) [42]	9.8	13.2
DFT (VASP) [43]	10.0	12.0
DFT (SIESTA) [44]	12.43	15.33
MM (REBO) [14]	10.91	10.41
MD (AIREBO) [This work]	11.63	10.81

4.2. Excess edge energy

Initial strain, discussed in section 4.1, arises due to the difference between the potential energies of edge and interior atoms. Figure 8 shows the variation of the average potential energy of atoms with the distance from the edge. Excess edge energy (γ) of armchair and zigzag sheets can be calculated as [14]

$$\gamma_{ac} = \frac{2\,(U_{a1} + U_{a2} - 2U_0)}{3r_0}, \qquad \gamma_{zz} = \frac{(U_{z1} + U_{z2} - 2U_0)}{\sqrt{3}r_0}, \tag{17}$$

where U_{a1}, U_{a2}, U_{z1} and U_{z2} are the average potential energies of edge atoms of armchair and zigzag sheets as labelled in figure 8; U_0 is the potential energy of an interior atom; and r_0 is the equilibrium C–C bond length of graphene.

The calculated γ_{ac} and γ_{zz} are well within the values reported in the literature, which are given in table 2. According to DFT methods, γ_{zz} is greater than γ_{ac}, whereas empirical potentials (REBO and AIREBO) give the opposite trend. The values calculated using the empirical potentials may be more accurate compared with those obtained from DFT, since empirical potentials use experimental data to fit some of the parameters in the potential [20], whereas DFT is purely theoretical. The values of γ, calculated in this work, might give a better approximation compared with the values found in [14] since the AIREBO potential considers the non-bonded and torsional interactions, which are not included in REBO potential used in [14].

4.3. Young's modulus and strength

Stress–strain curves of GNRs with various widths are obtained as explained in section 3. Figure 9 shows that edges have a significant effect on the stress–strain curves of GNRs. The armchair sheets show a significant variation in Young's modulus (E) with changing width, whereas the zigzag sheets show relatively minor changes, as indicated in figure 10. This may

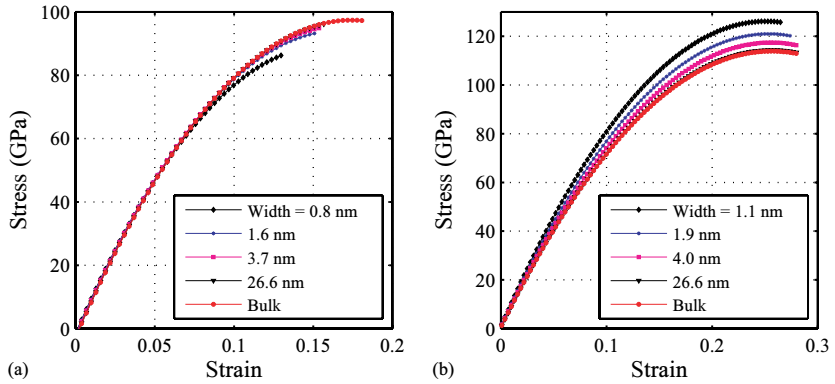

Figure 9. Stress–strain curves of (*a*) armchair and (*b*) zigzag GNRs at 1 K.

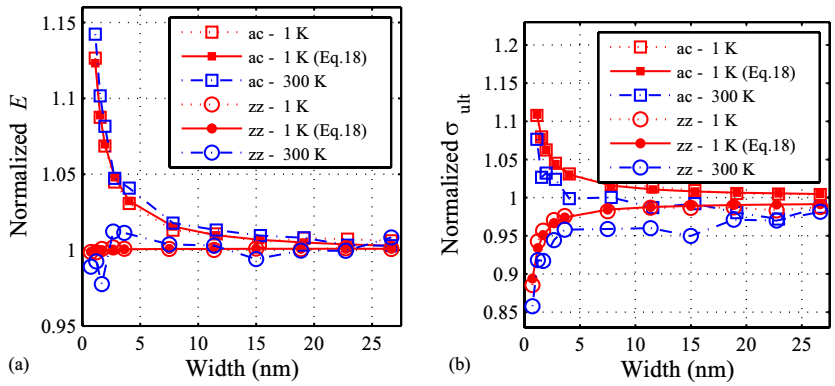

Figure 10. (*a*) Variation of Young's modulus (E) and (*b*) strength of GNRs with various widths at different temperatures. Young's modulus of armchair sheets has been normalized with respect to 0.884 TPa and 0.899 TPa at 1 K and 300 K, respectively. Respective values of zigzag are 1.148 TPa and 1.111 TPa. Strength of armchair sheets has been normalized with respect to 113.9 GPa and 107.5 GPa at 1 K and 300 K, respectively. Respective values of zigzag are 97.4 GPa and 90.6 GPa.

be due to the existence of bonds between unstable edge atoms in armchair sheets, which is not present in zigzag sheets. The bonds between unstable edge atoms could make the armchair sheets much weaker compared with zigzag sheets. However, narrow armchair sheets have higher E and σ_{ult} values compared with wider sheets. An investigation of the potential energy stored in individual atoms revealed that atoms next to armchair edges store a higher amount of potential energy than that of the zigzag edge [40], which could arise from the bonding environment of atoms. This causes narrow armchair sheets to have a higher E and σ_{ult}, since the effect of edge atoms is significant at narrow widths. The edge effects disappear as the sheets become wider than 10 nm. Temperature does not have a significant effect on E. σ_{ult} of the sheets slightly lower at 300 K compared with 1 K.

According to equation (15), E_{eff} and σ_{ult} of GNRs can be written as

$$E_{\text{eff}} = \frac{2E_s}{w} + E_{\text{b}}, \qquad \sigma_{\text{ult}} = \frac{2\sigma_{s,\text{ult}}}{w} + \sigma_{\text{b,ult}}, \tag{18}$$

where, E_{b} and $\sigma_{\text{b,ult}}$ are the Young's modulus and ultimate tensile strength of bulk graphene, respectively. Figure 10 shows that equation (18) fits well with the results obtained from MD

Table 3. Effects of temperature on properties of GNRs.

	Temp (K)	E_s (TPa nm)	E_b (TPa)	$\sigma_{s,ult}$ (GPa nm)	$\sigma_{s,ult}$ (GPa)
Armchair	1	0.062	0.882	6.93	113.9
	300	0.072	0.897	5.12	105.5
Zigzag	1	−0.001	1.149	−3.55	96.8
	300	−0.007	1.115	−3.84	88.5

simulations. The values of E_b, E_s, $\sigma_{b,ult}$ and $\sigma_{s,ult}$ are obtained from regression analysis and the corresponding values are given in table 3. The positive values of E_s of armchair edges increase E_{eff}, whereas E_s of zigzag edges are negligible. It can also be seen that the magnitude of E_s at 300 K is greater than that of the corresponding value at 1 K, which indicates that the edge effects could become significant at higher temperatures. A similar procedure was adapted to calculate E_s in [15] and they found that the values for the armchair and zigzag edges at 0 K are 0.011 TPa nm and 0.024 TPa nm, respectively. E_{eff} in [15] was obtained by fitting an eighth order polynomial between the strain energy and strain of GNRs. The strain energy–strain relation in this work is a third order polynomial, as revealed by experiments on graphene [5]. On the other hand, the simulations in [15] were conducted using the REBO potential whereas this work is carried out using the AIREBO potential. The change in E_{eff} with temperature was not studied in [15]. It can also be seen in table 3 that the effect of the armchair edge is greater than that of the zigzag, as indicated by the values of $\sigma_{s,ult}$. The armchair edge improves σ_{ult}, whereas the zigzag edge reduces it.

This paper has focussed on perfect graphene sheets and GNRs. The results presented here give an idea about the ideal strength that could be achieved in graphene-based devices. Researchers are making progress to fabricate defect-free graphene [1–3]. However, defects are unavoidable in many applications and they will considerably reduce the strength of graphene. Investigation on the interactions between defects and edges of GNRs is a future research endeavour.

5. Conclusions

We presented a comprehensive molecular dynamics (MD) simulation study on the effects of temperature and free edges on the Young's modulus and ultimate tensile strength of graphene sheets. It is found that sheets at higher temperatures fail at lower strains and that temperature does not influence the Young's modulus. A numerical model is proposed to calculate the temperature and strain-rate-dependent ultimate tensile strength and strain of graphene. It is also found that continuum stress definition gives a residual stress in infinite sheets at higher temperatures, whereas virial stress shows no residual stress. The initial out-of-plane displacement should be induced to the atoms when the Nosé–Hoover or Berendsen thermostat is used.

A study on the influence of edges shows that excess edge energy of graphene sheets induces the initial strain. The concept of surface stress of a three-dimensional crystal can be used to predict the initial strain with a high degree of accuracy. The excess edge energies calculated from MD simulations with the AIREBO potential agree quite well with the values obtained from molecular mechanics simulations with the REBO potential. Free edges have a greater influence on the Young's modulus and ultimate tensile strength of the zigzag sheets compared with that of the armchair sheets.

Acknowledgment

This research was supported by the Natural Sciences and Engineering Research Council (NSERC) of Canada and the Canada Research Chairs programme.

References

[1] Dikin D A, Stankovich S, Zimney E J, Piner R D, Dommett G H B, Evmenenko G, Nguyen S T and Ruoff R S 2007 Preparation and characterization of graphene oxide paper *Nature* **448** 457–460
[2] Ramanathan T *et al* 2008 Functionalized graphene sheets for polymer nanocomposites *Nature Nano* **3** 327–31
[3] Rafiee M A, Rafiee J, Srivastava I, Wang Z, Song H, Yu Z Z and Koratkar N 2010 Fracture and fatigue in graphene nanocomposites *Small* **6** 179–83
[4] Eswaraiah V, Balasubramaniam K and Ramaprabhu S 2012 One-pot synthesis of conducting graphene-polymer composites and their strain sensing application *Nanoscale* **4** 1258–62
[5] Lee C, Wei X, Kysar J W and Hone J 2008 Measurement of the elastic properties and intrinsic strength of monolayer graphene *Science* **321** 385–8
[6] Chen C, Rosenblatt S, Bolotin K I, Kalb W, Kim P, Kymissis I, Stormer H L, Heinz T F and Hone J 2009 Performance of monolayer graphene nanomechanical resonators with electrical readout *Nature Nanotechnol.* **4** 861–7
[7] Robinson J T, Zalalutdinov M, Baldwin J W, Snow E S, Wei Z, Sheehan P and Houston B H 2008 Wafer-scale reduced graphene oxide films for nanomechanical devices *Nano Lett.* **8** 3441–5
[8] Bunch J S, van der Zande A M, Verbridge S S, Frank I W, Tanenbaum D M, Parpia J M, Craighead H G and McEuen P L 2007 Electromechanical resonators from graphene sheets *Science* **315** 490–3
[9] Reserbat-Plantey A, Marty L, Arcizet O, Bendiab N and Bouchiat V 2012 A local optical probe for measuring motion and stress in a nanoelectromechanical system *Nature Nanotechnol.* **7** 151–5
[10] Burghard M, Klauk H and Kern K 2009 Carbon-based field-effect transistors for nanoelectronics *Adv. Mater.* **21** 2586–600
[11] Shenoy V B, Reddy C D, Ramasubramaniam A and Zhang Y W 2008 Edge-stress-induced warping of graphene sheets and nanoribbons *Phys. Rev. Lett.* **101** 245501
[12] Reddy C D, Ramasubramaniam A, Shenoy V B and Zhang Y W 2009 Edge elastic properties of defect-free single-layer graphene sheets *Appl. Phys. Lett.* **94** 101904
[13] Bu H, Chen Y, Zou M, Yi H, Bi K and Ni Z 2009 Atomistic simulations of mechanical properties of graphene nanoribbons *Phys. Lett.* A **373** 3359–62
[14] Lu Q and Huang R 2010 Excess energy and deformation along free edges of graphene nanoribbons *Phys. Rev.* B **81** 155410
[15] Lu Q, Gao W and Huang R 2011 Atomistic simulation and continuum modeling of graphene nanoribbons under uniaxial tension *Model. Simul. Mater. Sci. Eng.* **19** 054006
[16] Zhao H and Aluru N R 2010 Temperature and strain-rate dependent fracture strength of graphene *J. Appl. Phys.* **108** 064321
[17] Stuart S J, Tutein A B and Harrison J A 2000 A reactive potential for hydrocarbons with intermolecular interactions *J. Chem. Phys.* **112** 6472–86
[18] Plimpton S 1995 Fast parallel algorithms for short-range molecular dynamics *J. Comput. Phys.* **117** 1–19
[19] Grantab R, Shenoy V B and Ruoff R S 2010 Anomalous strength characteristics of tilt grain boundaries in graphene *Science* **330** 946–8
[20] Brenner D W 1990 Empirical potential for hydrocarbons for use in simulating the chemical vapor deposition of diamond films *Phys. Rev.* B **42** 9458
[21] Shenderova O A, Brenner D W, Omeltchenko A, Su X and Yang L H 2000 Atomistic modeling of the fracture of polycrystalline diamond *Phys. Rev.* B **61** 3877–88
[22] Ni Z, Bu H, Zou M, Yi H, Bi K and Chen Y 2010 Anisotropic mechanical properties of graphene sheets from molecular dynamics *Physica* B **405** 1301–6
[23] Pastewka L, Mrovec M, Moseler M and Gumbsch P 2012 Bond order potentials for fracture, wear, and plasticity *MRS Bull.* **37** 493–503
[24] Liu F, Ming P and Li J 2007 *Ab initio* calculation of ideal strength and phonon instability of graphene under tension *Phys. Rev.* B **76** 064120
[25] Hwang C, Yoo K, Kim S J, Seo E K, Yu H and Biró L P 2011 Initial stage of graphene growth on a Cu substrate *J. Phys. Chem.* C **115** 22369–74

[26] Bao W, Miao F, Chen Z, Zhang H, Jang W, Dames C and Lau C N 2009 Controlled ripple texturing of suspended graphene and ultrathin graphite membranes *Nature Nanotechnol.* **4** 562–6
[27] Fasolino A, Los J H and Katsnelson M I 2007 Intrinsic ripples in graphene *Nature Mater.* **6** 858–61
[28] Lui C H, Liu L, Mak K F, Flynn G W and Heinz T F 2009 Ultraflat graphene *Nature* **462** 339–41
[29] Singh V, Sengupta S, Solanki H S, Dhall R, Allain A, Dhara S, Pant P and Deshmukh M M 2010 Probing thermal expansion of graphene and modal dispersion at low-temperature using graphene nanoelectromechanical systems resonators *Nanotechnology* **21** 165204
[30] Schneider T and Stoll E 1978 Molecular-dynamics study of a three-dimensional one-component model for distortive phase transitions *Phys. Rev.* B **17** 1302–22
[31] Nosé S 1984 A molecular dynamics method for simulations in the canonical ensemble *Mol. Phys.* **52** 255–68
[32] Hoover W G 1985 Canonical dynamics: equilibrium phase-space distributions *Phys. Rev.* A **31** 1695–7
[33] Berendsen H J C, Postma J P M, van Gunsteren W F, DiNola A and Haak J R 1984 Molecular dynamics with coupling to an external bath *J. Chem. Phys.* **81** 3684
[34] Pozzo M, Alfè D, Lacovig P, Hofmann P, Lizzit S and Baraldi A 2011 Thermal expansion of supported and freestanding graphene: lattice constant versus interatomic distance *Phys. Rev. Lett.* **106** 135501
[35] Arrhenius S 1889 On the reaction rate of the inversion of the non-refined sugar upon souring *Z. Phys. Chem.* **4** 226–48
[36] Mylvaganam K and Zhang L 2004 Important issues in a molecular dynamics simulation for characterising the mechanical properties of carbon nanotubes *Carbon* **42** 2025–32
[37] Admal N and Tadmor E B 2010 A unified interpretation of stress in molecular systems *J. Elast.* **100** 63–143
[38] Clausius R 1870 XVI On a mechanical theorem applicable to heat *Phil. Mag. Ser. 4* **40** 122–7
[39] Tsai D H 1979 The virial theorem and stress calculation in molecular dynamics *J. Chem. Phys.* **70** 1375–82
[40] Dewapriya M A N 2012 Molecular dynamics study of effects of geometric defects on the mechanical properties of graphene *MASc Thesis* The University of British Columbia, Canada
[41] Cammarata R C 1994 Surface and interface stress effects in thin films. *Prog. Surf. Sci.* **46** 1–38
[42] Koskinen P, Malola S and Häkkinen H 2008 Self-passivating edge reconstructions of graphene *Phys. Rev. Lett.* **101** 115502
[43] Huang B, Liu M, Su N, Wu J, Duan W, Gu B and Liu F 2009 Quantum manifestations of graphene edge stress and edge instability: a first-principles study *Phys. Rev. Lett.* **102** 166404
[44] Jun S 2008 Density-functional study of edge stress in graphene *Phys. Rev.* B **78** 073405